Electron transport in nanoscale junctions with local anharmonic modes

Lena Simine and Dvira Segal

Chemical Physics Theory Group, Department of Chemistry,
University of Toronto, 80 Saint George St. Toronto, Ontario, Canada M5S 3H6
(Dated: July 4, 2018)

We study electron transport in nanojunctions in which an electron on a quantum dot or a molecule is interacting with an N-state local impurity, a harmonic ("Holstein") mode, or a two-state system ("spin"). These two models, the Anderson-Holstein model and the spin-fermion model, can be conveniently transformed by a shift transformation into a form suitable for a perturbative expansion in the tunneling matrix element. We explore the current-voltage characteristics of the two models in the limit of high temperature and weak electron-metal coupling using a kinetic rate equation formalism, considering both the case of an equilibrated impurity, and the unequilibrated case. Specifically, we show that the analog of the Franck-Condon blockade physics is missing in the spin-fermion model. We complement this study by considering the low-temperature quantum adiabatic limit of the dissipative spin-fermion model, with fast tunneling electrons and a slow impurity. While a mean-field analysis of the Anderson-Holstein model suggests that nonlinear functionalities, bistability and hysteresis may develop, such effects are missing in the spin-fermion model at the mean-field level.

I. INTRODUCTION

Molecular electronic devices have been of significant interest in the past decade offering a fertile playground for studying fundamentals of nonequilibrium many-body physics [1–3]. The simplest junction includes a single molecule, possibly gated, bridging two voltage-biased leads. Mechanisms of charge transport in such systems, specifically, the role of many-body interactions (electron-phonon, electron-electron, electron-magnetic impurity) can be resolved e.g., from direct current-voltage measurements, studies of current noise, and from different types of spectroscopy, inelastic electron tunneling spectroscopy and Raman studies [1–3]. Naturally, molecular electronic degrees of freedom are coupled to nuclear vibrations, and signatures of this interaction appear through peaks in the differential conductance [4], nonequilibrium heating of vibrational modes [5], the presence of the Franck-Condon blockade [6–9] and other (proposed) effects: vibrational instabilities [10–12], vibrationally induced negative differential resistance [13], current hysteresis, switching and bistability [14–20], and electron-pair tunneling [21].

In the simplest theoretical description of electron-conducting junctions only degrees of freedom that immediately participate in the transport process are included. The single-impurity "Anderson-Holstein" (AH) model comprises a single electronic level (dot) and a local harmonic-vibrational mode. Electrons on the dot may electrostatically repel, but the metals are treated as Fermi gases with noninteracting electrons. This minimal model has been revisited many times, and it has been examined in different limits by means of analytical, perturbative and numerical techniques. Perturbation expansions were performed in either the electron-phonon interaction parameter or the tunneling matrix element to the metals, resulting in Redfield [12, 13, 22], polaronic [7, 8, 11, 23] and Keldysh Green's function equations of motion [24]. Numerically exact tools provide transient effects towards the steady-state limit. Among such techniques we list wave-function based methodologies [19, 20, 25], time-dependent numerical renormalization group approaches [26, 27], and iterative-deterministic [28] and diagrammatic Monte Carlo [29, 30] path-integral tools.
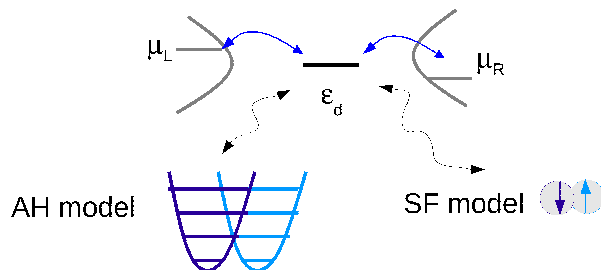

FIG. 1: Minimal modeling of nanojunctions with a single electronic level (energy ϵ_d) coupled to two metals. In the Anderson-Holstein (AH) model the vibrational mode is displaced depending on the charge number in the dot. The spin-fermion model (SF) is a truncated version of the AH model. Its (nondegenerate) two states describe e.g., an anharmonic mode or a magnetic impurity in an external magnetic field. Electrons residing on the dot may flip the spin state.

The Anderson-Holstein model describes the potential energy of atoms displaced from equilibrium within the harmonic approximation. It is important to examine nanojunctions beyond this ideal limit, and describe more realistic structures. Several recent studies considered the role of molecular anharmonicity (in the form of a Morse potential) on charge transport characteristics, generally displaying small effects [10, 31]. More fundamentally, the AH model should be extended beyond the harmonic limit to describe situations in which electrons on the dot couple

to naturally anharmonic degrees of freedom, intramolecular, or in the surrounding. Such situations arise in different setups: nanojunctions consisting local magnetic impurities [32, 33], nanoelectromechanical devices [34], semiconductor quantum dots coupled to nuclear spins in the surroundings [35–37], charge sensing in the junction through e.g., nitrogen-vacancy centers [38, 39], and when the electronic degrees of freedom are coupled to (discrete or continuous) molecular conformations [40].

In this paper we extend the AH model, and allow the electron on the dot to interact with an N-state "impurity", rather than with a strictly harmonic mode. Particularly, we introduce the "spin fermion" (SF) model with a two-state impurity, e.g. a magnetic spin, see Fig. 1. The AH and the SF models were treated separately in the literature in the context of molecular electronics, or in relation to the nonequilibrium Kondo physics. The purpose of this paper is to provide a direct comparison between the transport characteristics of these two situations, with very simple modeling. Our goal is to explore whether nontrivial nonequilibrium many-body effects predicted to show in the AH model: Franck-Condon blockade and current hysteresis and bistability, persist when the dot electron interacts with a different type of a scatterer, e.g., a magnetic spin.

We compare the behavior of the AH and SF models in two limits. First, at high temperatures we use a simple-transparent rate equation method [7, 11, 23]. Applying a general small-polaron-type transformation, we reduce the N-state impurity model Hamiltonian into a form suitable for a strong-coupling electron-impurity treatment. We then study the current-voltage characteristics of the AH and the SF models in the sequential-tunneling limit, and explore current blockade mechanisms. We confirm that in the AH model the Franck-Condon blockade (FCB) effect dominates at strong coupling [6, 7], but we find that in the SF model this type of blockade is missing altogether. In the second part of the paper we briefly compare the behavior of the two models in the quantum regime, in the complementary adiabatic limit (fast electrons and a slow impurity). Particularly, we examine the possible existence of bistability and hysteresis in the SF model. In this limit we find that the transport characteristics of the SF and AH models directly correspond, but that such nonlinear effects, predicted to show up for the AH model, are missing in the SF case.

The paper is organized as follows: In Sec. II, we introduce the general model Hamiltonian and the two examples: the AH (Sec. II B) and the SF models (Sec. II C). We also discuss these models in the broader context of transport in a tight-binding network (Appendix). In Sec. III we study the current-voltage characteristics in the nonadiabatic limit. We review the master equation methodology in Sec. III A, and discuss the case with dissipation in Sec. III B. Numerical results are presented in Sec. III C. In Sec. IV we discuss the complementary quantum-adiabatic regime of strong electron-metal coupling and a slow impurity. Sec. V concludes. For

simplicity, we set $\hbar = 1$, $k_B = 1$ (Boltzmann constant), and $e = 1$ throughout the paper.

II. MODEL

A. N-state impurity

Our simple modeling of a molecular junction consists a single spin-degenerate molecular electronic level (dot) of energy ϵ_d. The dot is tunnel-coupled to two voltage-biased metallic contacts. In the standard Anderson-Holstein model electrons on the dot interact with equilibrated or unequilibrated harmonic vibrational modes. We generalize this setup and allow the electron to interact with an N-state unit: spin qubit ($N = 2$), large spin ($N > 2$), harmonic oscillator ($N \to \infty$) or an anharmonic mode with a finite number of bound states. We refer below to this N-state entity as an "impurity", and incorporate it in the system-molecular Hamiltonian H_S. The total Hamiltonian comprises the following terms

$$H = H_S + H_B + H_{SB}. \tag{1}$$

The system Hamiltonian includes the molecular electronic level (creation operator $d^\dagger$), the N-state impurity, and the dot-impurity interaction,

$$H_S = \epsilon_d \hat{n}_d + \sum_{q=0}^{N-1} \epsilon_q |q\rangle\langle q| + \alpha \hat{n}_d \sum_{q,q'} F_{q,q'} |q\rangle\langle q'|. \tag{2}$$

Here $\hat{n}_d = d^\dagger d$ denotes the occupation number operator for the dot. The impurity Hamiltonian is written in the energy representation with the (possibly many-body) states $|q\rangle$, $q, q' = 0, 1, ..., N-1$. It is coupled to the electron via its operator F with matrix elements $F_{q,q'}$, α is a dimensionless parameter. The bath includes two conductors ($\nu = L, R$) comprising noninteracting fermions with creation (annihilation) operators $a^\dagger_{\nu,k}$ ($a_{\nu,k}$),

$$H_B = \sum_{\nu,k} \epsilon_k a^\dagger_{\nu,k} a_{\nu,k}. \tag{3}$$

The system-bath coupling includes the tunneling Hamiltonian,

$$H_{SB} = \sum_{\nu,k} \left(v_{\nu,k} a^\dagger_{\nu,k} d + v^*_{\nu,k} d^\dagger a_{\nu,k} \right), \tag{4}$$

with $v_{\nu,k}$ as the tunneling element, introducing the hybridization energy

$$\Gamma_\nu(\epsilon) = 2\pi \sum_k |v_{\nu,k}|^2 \delta(\epsilon - \epsilon_k). \tag{5}$$

The Hamiltonian (1)-(4) can be transformed into a form more suitable for a perturbative expansion in the tunneling matrix element by means of a unitary-shift transformation. It is useful to define the impurity Hamiltonian,

$H_{imp} = H_S(\hat{n}_d = 1)$, or explicitly

$$H_{imp} = \sum_q \epsilon_q |q\rangle\langle q| + \alpha \sum_{q,q'} F_{q,q'} |q\rangle\langle q'|. \qquad (6)$$

This operator is hermitian and it can be diagonalized with a unitary transformation

$$\bar{H}_{imp} = e^A H_{imp} e^{-A}, \qquad (7)$$

where $A^\dagger = -A$ is an anti-hermitian operator in the Hilbert space of the N-state impurity. We now introduce a related unitary operator, $V \equiv e^{A\hat{n}_d}$. Note that $e^{A\hat{n}_d} d e^{-A\hat{n}_d} = d e^{-A}$ and $e^{A\hat{n}_d} d^\dagger e^{-A\hat{n}_d} = d^\dagger e^A$. Thus, operating on the original Hamiltonian, $\bar{H} = VHV^\dagger$, we reach

$$\begin{aligned}
\bar{H} =\ & \sum_{\nu,k} \epsilon_k a^\dagger_{\nu,k} a_{\nu,k} + \epsilon_d \hat{n}_d \\
& + \sum_{\nu,k} \left(v_{\nu,k} a^\dagger_{\nu,k} d e^{-A} + v^*_{\nu,k} d^\dagger a_{\nu,k} e^A \right) \\
& + (1 - \hat{n}_d) \sum_q \epsilon_q |q\rangle\langle q| + \hat{n}_d \bar{H}_{imp}.
\end{aligned} \qquad (8)$$

We now exemplify this transformation in two limits. In the standard AH model the impurity corresponds to a harmonic mode which is coupled through its displacement to the dot. In the SF model the impurity includes two states, and the two-state transition operator is coupled to the dot number operator. Furthermore, the transformation can be performed on a tight-binding model with M electronic sites, where each site is coupled to multiple impurities. In the Appendix we discuss this extension in the context of exciton transfer in chromophore complexes, considering an anharmonic environment rather than the common harmonic-bath model [47, 48].

B. Case I: Harmonic oscillator

The AH Hamiltonian follows the generic form (2)-(4), specified as

$$H_{AH} = H_S^{AH} + H_B + H_{SB}. \qquad (9)$$

The excess electron on the dot interacts with an harmonic mode of frequency ω_0, $\epsilon_q = q\omega_0$, $q = 0, 1, 2, ...$, sometimes referred to as a "phonon". The interaction operator allows excitation and de-excitation processes between neighboring vibrational states,

$$F_{q,q'} = \omega_0 \sum_{q,q'} \sqrt{q} |q\rangle\langle q'| \delta_{q'=q-1} + h.c. \qquad (10)$$

It is more convenient to work with the creation and annihilation operators, $b_0^\dagger$ and b_0, for a boson mode of frequency ω_0. The molecular Hamiltonian is given by

$H_S^{AH} = \omega_0 b_0^\dagger b_0 + \alpha\omega_0 \left(b_0^\dagger + b_0 \right) \hat{n}_d$, and the impurity Hamiltonian

$$H_{imp}^{AH} = \omega_0 b_0^\dagger b_0 + \alpha\omega_0 \left(b_0^\dagger + b_0 \right) \qquad (11)$$

can be diagonalized with the (small-polaron) shift transformation (7) [41]. The operator A satisfies

$$A = \alpha(b_0^\dagger - b_0), \qquad (12)$$

resulting in

$$\bar{H}_{imp}^{AH} = \omega_0 b_0^\dagger b_0 - \alpha^2 \omega_0. \qquad (13)$$

We substitute this expression into Eq. (8), and immediately obtain the standard result

$$\begin{aligned}
\bar{H}_{AH} =\ & e^{A\hat{n}_d} H_{AH} e^{-A\hat{n}_d} \\
=\ & \sum_{\nu,k} \epsilon_k a^\dagger_{\nu,k} a_{\nu,k} \\
& + \sum_{\nu,k} \left[v_{\nu,k} a^\dagger_{\nu,k} d e^{-\alpha(b_0^\dagger - b_0)} + v^*_{\nu,k} d^\dagger a_{\nu,k} e^{\alpha(b_0^\dagger - b_0)} \right] \\
& + \epsilon_d \hat{n}_d + \omega_0 b_0^\dagger b_0 - \alpha^2 \omega_0 \hat{n}_d.
\end{aligned} \qquad (14)$$

The interaction of electrons with phonons form the "polaron": The single-particle dot energies are renormalized, $\epsilon_d \to \epsilon_d - \alpha^2 \omega_0$, and the tunneling elements are dressed by the translational operator $e^{-\alpha(b_0^\dagger - b_0)}$, corresponding to a shift in the equilibrium position of the mode when an electron is residing on the dot.

C. Case II: Two-level system

In the "spin-fermion model" the excess electron on the dot is coupled to a two-state system, referred to as a "spin". This model has been explored in previous works, for example in Refs. [42–45], but focus has been placed on the decoherence and dissipative dynamics of the two-level system, specifically when interacting with a nonequilibrium environment, voltage-biased leads. Complementing these studies, here we investigate the transport characteristics of the SF model. The total Hamiltonian (2)-(4) now reads

$$H_{SF} = H_S^{SF} + H_B + H_{SB}, \qquad (15)$$

with the molecular part $H_S^{SF} = \frac{\omega_0}{2}\sigma_z + \alpha\omega_0\sigma_x\hat{n}_d$. Here, $\sigma_{x,y,z}$ denote the Pauli matrices. The impurity Hamiltonian is hermitian,

$$H_{imp}^{SF} = \frac{\omega_0}{2}\sigma_z + \alpha\omega_0\sigma_x, \qquad (16)$$

and it can be diagonalized with a unitary transformation (7). The generator of this transformation is

$$A = i\lambda\sigma_y, \quad \lambda = \frac{1}{2}\arctan(2\alpha), \qquad (17)$$

resulting in

$$\bar{H}_{imp}^{SF} = \frac{\omega_0}{2}\sigma_z + \frac{\omega_0}{2}\left(\frac{1-\cos 2\lambda}{\cos 2\lambda}\right)\sigma_z. \qquad (18)$$

We substitute this expression into Eq. (8) and reach

$$
\begin{aligned}
\bar{H}_{SF} &= e^{A\hat{n}_d}H_{SF}e^{-A\hat{n}_d} \\
&= \sum_{\nu,k}\epsilon_k a_{\nu,k}^\dagger a_{\nu,k} \\
&\quad + \sum_{\nu,k}\left[v_{\nu,k}a_{\nu,k}^\dagger d e^{-i\lambda\sigma_y} + v_{\nu,k}^* d^\dagger a_{\nu,k}e^{i\lambda\sigma_y}\right] \\
&\quad + \epsilon_d\hat{n}_d + \frac{\omega_0}{2}\sigma_z + \frac{\omega_0}{2}\left(\frac{1-\cos 2\lambda}{\cos 2\lambda}\right)\sigma_z\hat{n}_d. \quad (19)
\end{aligned}
$$

A related shift transformation has been used in Ref. [46] for studying the dynamics of a spin immersed in a spin bath within the noninteracting blip approximation.

Recall that in the shifted AH model, Eq. (14), electron-phonon coupling shows up in two (polaronic) features: the dot-metal tunneling elements are dressed, and the single particle (dot) energies are renormalized. In the SF model (19) the tunneling operators are similarly dressed by the interaction parameter λ, a nonlinear function of the original dimensionless coupling α. Furthermore, the SF model displays an anharmonic characteristic: the spin gap (energy bias) depends on the charge state of the dot.

III. KINETIC EQUATIONS FOR $\Gamma_\nu < \omega_0, T_\nu$

In this section we study the current-voltage characteristics of the AH and SF models of Sec. II B and II C in the classical high-temperature limit and weak dot-metal coupling by using the kinetic rate equation method of Refs. [7, 8, 11, 23].

A. Unequilibrated impurity

The shifted Hamiltonian, Eq. (14) or Eq. (19), can be compacted into the form $\bar{H} = H_B + \bar{H}_{SB} + \bar{H}_S$; $\bar{H}_{SB}$ includes the dressed tunnel Hamiltonian, $\bar{H}_S$ constitutes the dot electron and the impurity, the last three terms in either Eq. (14) or (19). The total Hamiltonian is given in a form conductive for a perturbative expansion in the electronic tunnel coupling $v_{\nu,k}$, and we now briefly review the derivation of a quantum Master equation valid to the lowest order in this parameter, while exact, to that order, in the impurity-electron coupling. In the absence of the leads the eigenstates of the molecular system satisfy

$$\bar{H}_S|n,q\rangle = \epsilon_{n,q}|n,q\rangle, \qquad (20)$$

where $n = 0, 1$ denotes the number of electrons on the dot and q identifies the state of the impurity. In the AH

model [Eq. (14)], $q = 0, 1, 2, ...$ counts the number of excited vibrations and the eigenenergies of $\bar{H}_S$ obey

$$
\begin{aligned}
\epsilon_{0,q} &= q\omega_0, \\
\epsilon_{1,q} &= \epsilon_d - \alpha^2\omega_0 + q\omega_0. \qquad (21)
\end{aligned}
$$

In the SF model [Eq. (19)] $q = \pm$ identifies the state of the spin. There are four possible molecular eigenstates with energies

$$
\begin{aligned}
\epsilon_{0,q} &= q\frac{\omega_0}{2}, \\
\epsilon_{1,q} &= \epsilon_d + q\frac{\omega_0}{2}(1+\kappa). \qquad (22)
\end{aligned}
$$

Here $\kappa = (1-\cos 2\lambda)/\cos 2\lambda$. Recall that $\lambda = \frac{1}{2}\arctan(2\alpha)$, with α as the original (dimensionless) electron-impurity interaction parameter. Simple manipulations provide $\kappa = \sqrt{1+4\alpha^2} - 1$, resulting in $\epsilon_{1,q} = \epsilon_d + q\frac{\omega_0}{2}\sqrt{1+4\alpha^2}$.

One can rigorously derive kinetic quantum master equations for the occupation P_q^n of the $|n, q\rangle$ state when the metal-molecule coupling is weak, $\Gamma_\nu < T_\nu, \omega_0$. The standard derivation is worked out from the quantum Liouville equation by applying the Born-Markov approximation, assuming fast electronic relaxation in the metals and slow tunneling dynamics. The resulting (bath-traced) reduced-density matrix ρ_S obeys [49, 50]

$$
\begin{aligned}
\dot{\rho}_S &= -i\mathrm{tr}_B[\bar{H}_{SB}(t), \rho_S(0)\rho_B] \\
&\quad - \mathrm{tr}_B\int_0^t d\tau[\bar{H}_{SB}(t), [\bar{H}_{SB}(\tau), \rho_S(t)\rho_B]], \quad (23)
\end{aligned}
$$

with ρ_B as the initial state of the two baths (metals), assumed to be given by a factorized form, with each bath prepared in a thermodynamic equilibrium state at the temperature β_ν^{-1} and a chemical potential μ_ν. The operators are written in the interaction representation and the trace is performed over the states of both baths. Applying the second part of the Markov limit, extending the upper limit of integration to infinity, this differential equation reduces to the Redfield equation [49]. It can be furthermore simplified under the secular approximation, ignoring coherences between molecular eigenstates. The result is an equation of motion for the diagonal elements of the reduced density matrix, $P_q^n(t) \equiv \langle q, n|\rho_S(t)|n, q\rangle$ [7, 11, 23],

$$\dot{P}_q^n(t) = \sum_{n',q'}\left(P_{q'}^{n'}w_{q'\to q}^{n'\to n} - P_q^n w_{q\to q'}^{n\to n'}\right), \qquad (24)$$

with $w_{q\to q'}^{n\to n'}$ as the rate constants for the $|n, q\rangle \to |n', q'\rangle$ transition. Processes that maintain the occupation state of the dot do not contribute in this low order sequential-tunneling scheme. Furthermore, the rate constants are additive in this expansion, $w_{q\to q'}^{n\to n'} = \sum_{\nu=L,R} w_{q\to q',\nu}^{n\to n'}$ with the ν-bath-induced rates satisfying

$$
\begin{aligned}
w_{q\to q',\nu}^{0\to 1} &= s(0,1)\Gamma_\nu f_\nu(\epsilon_{1,q'} - \epsilon_{0,q})|M_{q,q'}|^2 \\
w_{q\to q',\nu}^{1\to 0} &= s(1,0)\Gamma_\nu\left[1 - f_\nu(\epsilon_{1,q} - \epsilon_{0,q'})\right]|M_{q,q'}|^2 (25)
\end{aligned}
$$

While we had omitted the identifier to the spin state of electrons in the original Hamiltonian, assuming electronic energies are spin degenerate, the transition rates can be amended to account for the multiplicity of the $n = 1$ level, by introducing the factors $s(0,1) = 2$ and $s(1,0) = 1$ [23]. The electronic hybridization is defined in Eq. (5), and it is assumed from now on to be energy independent. The function $f_\nu(\epsilon) = [e^{\beta_\nu(\epsilon-\mu_\nu)}+1]^{-1}$ denotes the Fermi-Dirac distribution of the ν lead. The matrix elements

$$M_{q,q'} = \langle q|e^{-A}|q'\rangle \qquad (26)$$

develop from the shift operators decorating the tunneling elements in Eq. (8). In the AH model these are the familiar Franck-Condon (FC) factors [51],

$$M_{q,q'}^{AH} \equiv \langle q|e^{-\alpha(b_0^\dagger-b_0)}|q'\rangle \quad q,q' = 0,1,2... \qquad (27)$$

$$= sign(q'-q)^{q-q'}\alpha^{q_M-q_m}e^{-\alpha^2/2}\sqrt{\frac{q_m!}{q_M!}}L_{q_m}^{q_M-q_m}(\alpha^2),$$

with $q_m = \min\{q,q'\}$, $q_M = \max\{q,q'\}$, and $L_a^b(x)$ as the generalized Laguerre polynomials. In the SF model [Eq. (19)] this matrix elements are given by ($q = \pm 1$)

$$M_{q,q'}^{SF} \equiv \langle q|e^{-i\lambda\sigma_y}|q'\rangle, \qquad (28)$$
$$M_{q,-q}^{SF} = -q\sin\lambda, \quad M_{q,q}^{SF} = \cos\lambda.$$

Recall, $\lambda = \frac{1}{2}\arctan(2\alpha)$. The electron current at the ν contact can be evaluated within the rate equation formalism at the sequential-tunneling limit [11],

$$I_\nu = \sum_{q,q'}\left(P_q^0 w_{q\to q',\nu}^{0\to 1} - P_q^1 w_{q\to q',\nu}^{1\to 0}\right). \qquad (29)$$

The correct dimensionality is reached by recovering the prefactor $e/\hbar$. Eq. (24) can be readily solved in the long time limit enforcing $\dot{P}_q^n = 0$. Substituting the resulting occupations into Eq. (29), one can confirm that in steady-state $I \equiv I_L = -I_R$. Our numerical results below display only steady-state properties. The formalism discussed here accounts only for sequential-tunneling processes, but it can be extended without much effort to accommodate next-order (co-tunneling) terms [7, 8]. One can also generalize this approach and calculate current noise [6, 7] and other high order cumulants through a full counting statistics analysis [52, 53].

B. Thermally-equilibrated or dissipative impurity

Interaction of the molecular junction with other degrees of freedom (DOF), solvent, secondary vibrations in the case of a of molecular junction, nuclear spins, the vibrations in the leads, may further influence the electronic current. We collect these DOF into an "environment" and assume that it constitutes a secondary effect for electrons while it directly dissipates the impurity. We

include this secondary environment in two different ways: (i) by enforcing the impurity to equilibrate with an additional bath of temperature $T_h = \beta_h^{-1}$, see Eq. (31) below, or (ii) by explicitly coupling the impurity to a large collection of DOF, noninteracting harmonic oscillators or spins.

Equilibrated impurity. The impurity is enforced to equilibrate with a heat bath at $T_h = \beta_h^{-1}$ by enforcing the ansatz [11],

$$P_q^n = P^n\frac{e^{-\beta_h\epsilon_{0,q}}}{\sum_q e^{-\beta_h\epsilon_{0,q}}}. \qquad (30)$$

We place this expression in Eq. (24), to solve for the corresponding electronic occupations ($P^1 = 1 - P^0$). In steady-state we find

$$P^0 = \frac{\sum_{q,q'}e^{-\beta_h\epsilon_{0,q'}}\omega_{q'\to q}^{1\to 0}}{\sum_{q,q'}\left(e^{-\beta_h\epsilon_{0,q'}}\omega_{q'\to q}^{1\to 0} + e^{-\beta_h\epsilon_{0,q}}\omega_{q\to q'}^{0\to 1}\right)}. \qquad (31)$$

The electronic occupations are substituted back into Eq. (30) to directly provide the charge current (29).

Dissipative impurity. We augment the AH Hamiltonian (9) with a heat heat comprising independent DOF, harmonic oscillators (bosonic operators $b_j^\dagger$, b_j) bilinearly coupled (interaction energy η_j) to the molecular vibration (bosonic operators $b_0^\dagger$, b_0),

$$\begin{aligned}H_{AH}^{diss} &= \sum_{\nu,k}\epsilon_k a_{\nu,k}^\dagger a_{\nu,k} + \sum_{\nu,k}\left(v_{\nu,k}a_{\nu,k}^\dagger d + v_{\nu,k}^* d^\dagger a_{\nu,k}\right) \\ &+ \omega_0 b_0^\dagger b_0 + \alpha\omega_0\left(b_0^\dagger + b_0\right)\hat{n}_d + \epsilon_d\hat{n}_d \\ &+ \sum_j\omega_j b_j^\dagger b_j + \left(b_0^\dagger + b_0\right)\sum_j\eta_j\left(b_j^\dagger + b_j\right)\end{aligned} \qquad (32)$$

Employing the small polaron transformation as discussed in Sec. II B, $\bar{H}_{AH}^{diss} = e^{A\hat{n}_d}H_{AH}^{diss}e^{-A\hat{n}_d}$ with $A = \alpha(b_0^\dagger - b_0)$, using the relations $e^{A\hat{n}_d}b_0^\dagger e^{-A\hat{n}_d} = b_0^\dagger - \alpha\hat{n}_d$ and $e^{A\hat{n}_d}b_0 e^{-A\hat{n}_d} = b_0 - \alpha\hat{n}_d$, we get

$$\begin{aligned}\bar{H}_{AH}^{diss} &= \sum_{\nu,k}\epsilon_k a_{\nu,k}^\dagger a_{\nu,k} + \sum_j\omega_j b_j^\dagger b_j \\ &+ \sum_{\nu,k}\left[v_{\nu,k}a_{\nu,k}^\dagger de^{-\alpha(b_0^\dagger-b_0)} + v_{\nu,k}^* d^\dagger a_{\nu,k}e^{\alpha(b_0^\dagger-b_0)}\right] \\ &+ \epsilon_d\hat{n}_d + \omega_0 b_0^\dagger b_0 - \alpha^2\hat{n}_d\omega_0 \\ &+ \left(b_0^\dagger + b_0 - 2\alpha\hat{n}_d\right)\sum_j\eta_j\left(b_j^\dagger + b_j\right).\end{aligned} \qquad (33)$$

In this form, the dot electron directly interacts with the phonon environment; this effect is small (as expected) when $\alpha \ll 1$.

In the same spirit the SF model can be extended to include a thermal environment, a harmonic bath or a

collection of spins. In the latter case it is written as

$$
\begin{aligned}
H_{SF}^{diss} &= \sum_{\nu,k}\epsilon_k a_{\nu,k}^\dagger a_{\nu,k} + \sum_{\nu,k}\left(v_{\nu,k}a_{\nu,k}^\dagger d + v_{\nu,k}^* d^\dagger a_{\nu,k}\right) \\
&+ \frac{\omega_0}{2}\sigma_z + \alpha\omega_0\sigma_x\hat{n}_d + \epsilon_d\hat{n}_d \\
&+ \sum_j \frac{\omega_j}{2}\sigma_z^j + \sigma_x\sum_j \eta_j\sigma_x^j.
\end{aligned} \tag{34}
$$

Applying the shift transformation of Sec. II C, we arrive at the form

$$
\begin{aligned}
\bar{H}_{SF}^{diss} &= \sum_{\nu,k}\epsilon_k a_{\nu,k}^\dagger a_{\nu,k} + \sum_j \frac{\omega_j}{2}\sigma_z^j \\
&+ \sum_{\nu,k}\left[v_{\nu,k}a_{\nu,k}^\dagger d e^{-i\lambda\sigma_y} + v_{\nu,k}^* d^\dagger a_{\nu,k} e^{i\lambda\sigma_y}\right] \\
&+ \epsilon_d\hat{n}_d + \frac{\omega_0}{2}\sigma_z + \frac{\omega_0}{2}\left(\frac{1-\cos 2\lambda}{\cos 2\lambda}\right)\sigma_z\hat{n}_d \\
&+ [\sigma_x\cos(2\lambda\hat{n}_d)+\sigma_z\sin(2\lambda\hat{n}_d)]\sum_j\eta_j\sigma_x^j
\end{aligned} \tag{35}
$$

The last term has been obtained by using the relation

$$
e^{i\lambda\hat{n}_d\sigma_y} = \cos(\lambda\hat{n}_d) + i\sigma_y\sin(\lambda\hat{n}_d). \tag{36}
$$

It can be simplified with the identities $\sin(2\lambda\hat{n}_d) = \hat{n}_d\sin 2\lambda$ and $\cos(2\lambda\hat{n}_d) = \hat{n}_d\cos 2\lambda + (1-\hat{n}_d)$.

The current-voltage characteristics of the dissipative models can be readily obtained in the sequential-tunneling limit by extending the rate equation treatment of Sec. III A, to include a weakly-coupled additional environment. For example, considering the SF model (35), the rate equation (24) becomes ($q, q' = \pm$),

$$
\begin{aligned}
\dot{P}_q^n(t) &= \sum_{n',q'}\left(P_{q'}^{n'}w_{q'\to q}^{n'\to n} - P_q^n w_{q\to q'}^{n\to n'}\right) \\
&+ \sum_{q'\neq q}\left(P_{q'}^n k_{q'\to q}^{n\to n} - P_q^n k_{q\to q'}^{n\to n}\right),
\end{aligned} \tag{37}
$$

with the metal-induced rates $w_{q\to q'}^{n\to n'}$ as in Eq. (25), and the heat-bath induced rates

$$
k_{q\to q'}^{n\to n} = \Gamma_h(\omega_0)n_S[(q'-q)\omega_0][1-n+n\cos(2\lambda)]. \tag{38}
$$

Here and in Eq. (40) below the spectral density function,

$$
\Gamma_h(\omega_0) = 2\pi\sum_j \eta_j^2\delta(\omega_j - \omega_0), \tag{39}
$$

is evaluated at the impurity energy spacing. To be consistent with the derivation of the kinetic equation (37), this interaction energy should be assumed small, $\Gamma_h \ll \alpha\omega_0$. The spin distribution function $n_S(\omega_0) = [e^{\beta_h\omega_0} + 1]^{-1}$ obeys the relation $n_S(-\omega_0) = 1 - n_S(\omega_0)$. We could similarly couple the spin impurity to a harmonic heat bath, modeling a secondary normal mode environment. In this

case the same rate equation holds, but the nonzero heat-bath induced rates obey

$$
k_{q\to q'}^{n\to n} = \Gamma_h(\omega_0)n_B[(q'-q)\omega_0], \tag{40}
$$

The Bose-Einstein distribution function $n_B(\omega_0) = [e^{\beta_h\omega_0} - 1]^{-1}$ satisfies $n_B(-\omega_0) = n_B(\omega_0) + 1$. The current [Eq. (29)] is computed from the long time solution of Eq. (37).

C.   Results

We study the behavior of the junction in the steady-state limit, and compare the current-voltage characteristics of the AH and SF models. Particularly, we wish to understand mechanisms of current suppression in these junctions. Unless otherwise stated, we used $\Gamma \equiv \Gamma_L = \Gamma_R$, $\beta_L = \beta_R = 20$, $\omega_0 = 1$. The voltage bias is applied symmetrically, $\mu_L = -\mu_R$, defining $\Delta\mu = \mu_L - \mu_R$. The current is given in units of Γ; the voltage bias $\Delta\mu$, Γ_h and T_ν, T_h are given in multiples of ω_0.

1.   Molecular eigenenergies and overlap integral

We present in Fig. 2 the eigenenergies of the molecular eigenstates $|n,q\rangle$, Eqs. (21) and (22). For simplicity, we include only six levels for the harmonic oscillator. The energies which do not develop with α correspond to an empty dot, $n = 0$. When an electron is residing on the molecule, the eigenenergies of the two models show marked qualitative differences: In the AH model energy spacings between adjacent levels are fixed, $\epsilon_{n,q} - \epsilon_{n,q-1} = \omega_0$, and the levels bend in a quadratic manner, see Eq. (21). In contrast, in the SF model the pair with $n = 1$ depart; at small α the departure is quadratic, $\epsilon_{1,+} - \epsilon_{1,-} \sim \alpha^2\omega_0$, while for large coupling the gap grows linearly with α. In Fig. 2 We display results using different gate voltages, ϵ_d, to assist us in explaining transport features below.

The dressing elements of the tunneling Hamiltonian are displayed in Fig. 3. In the AH model (dashed lines) $\langle q|e^{-\alpha(b_0^\dagger - b_0)}|0\rangle$ are the common Franck-Condon (FC) factors, overlap integrals between the ground vibronic state and excited vibronic levels. We can interpret the dressing terms of the SF model (full lines) by considering, for example, the element $\langle\pm|e^{-i\lambda\sigma_y}|+\rangle$. Note that when $\alpha \to \infty$, $\lambda \to \pi/4$ and $|\sin(\lambda)|^2 = |\cos\lambda|^2 = 1/2$. The spin-up state can thus be rotated by an angle $\lambda \leq \pi/4$ to produce

$$
e^{-i\lambda\sigma_y}|+\rangle = \cos\lambda|+\rangle + \sin\lambda|-\rangle. \tag{41}
$$

We then overlap the shifted state with the two possible spin outcomes. We learn from Fig. 3 that while in the AH model the FC factors favor high energy transitions at large α, to realize the Franck-Condon blockade

physics, in the SF model this effect is missing and transitions which do not involve a spin-flip are favored for all α. What about other nanojunctions, with $N > 2$ impurities? In Fig. 4 we consider truncated (finite N) harmonic impurities satisfying Eqs. (6) and (10). We display the matrix elements $M_{0,q}$ obtained from Eq. (26), where e^A is the unitary transformation diagonalizing the relevant impurity Hamiltonian. We find that already for $N = 3$ off-diagonal transitions are favored at large α, once the curves cross and $|M_{0,0}|^2 < |M_{0,1}|^2$. We have also verified (not shown) that for large N we recover the standard FC elements.

2. Mechanisms of current blockade

Current blockade, suppression of electronic current for voltage biases below a certain critical value, may develop through different mechanisms: (i) In noninteracting models or for weakly-interacting cases the tunneling current is suppressed in off-resonance situations. We now elaborate on this trivial suppression, then clarify the related many-body case. Ignoring interactions, the AH and SF models reduce to the resonant-level model. The steady-state current can now be calculated exactly, and this Landauer expression can be expanded in orders of Γ_ν / T_ν to provide the lowest order sequential-tunneling limit

$$I = \frac{\Gamma_L \Gamma_R}{\Gamma_L + \Gamma_R} \left[f_L(\epsilon_d) - f_R(\epsilon_d) \right]. \tag{42}$$

If the resonant level, energy ϵ_d, is placed outside the bias window, an "off-resonance blockade" (ORB) (current suppression) shows. At positive bias the blockade is lifted at the critical voltage $\Delta\mu_c$ satisfying (the Fermi energy is set to zero),

$$\Delta\mu_c = 2|\epsilon_d|. \tag{43}$$

FIG. 3: Dressing elements $|M_{q,q'}|^2$ in the AH model following Eq. (28) with $q = 0$ and $q' = 0, 1, 2$ (dashed lines, left to right), and in the SF model following Eq. (29), $q, q' = \pm 1$ (full). $\omega_0 = 1$.
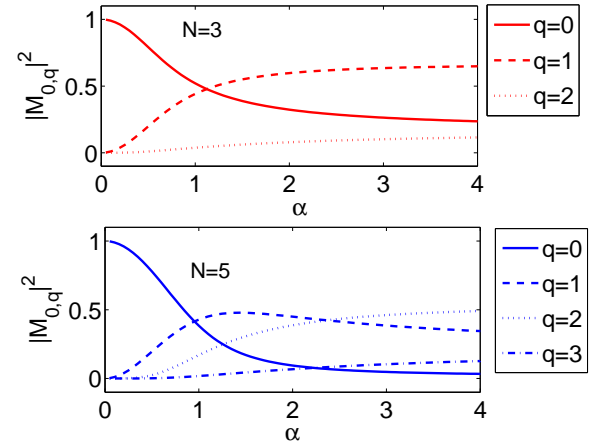
FIG. 4: Dressing elements $|M_{q,q'}|^2$ for truncated harmonic impurities of $N = 3$ and $N = 5$ states with $F_{q,q'}$ from Eq. (10).

In strongly interacting systems this off-resonance condition is modified by the many-body interaction parameter α. In general terms, the blockade is lifted when the applied bias is large so as incoming electrons can provide sufficient energy for making (allowed) transitions between many-body states, within the relevant order of perturbation theory,

$$\Delta\mu_c = 2\Delta E, \quad \Delta E \equiv min|\epsilon_{1,q} - \epsilon_{0,q'}|. \tag{44}$$

We refer below to this many-body extension of the ORB as the "many-body off-resonance blockade" (MB-ORB). One should note that this effect takes place in both the SF and the AH models.

At low temperatures $T_h/\omega_0 \ll 1$ only the ground state of the impurity is significantly occupied. The blockade is then practically determined by a pair of states which are thermally occupied, not necessarily of the smallest frequency (44). For example, in the SF model the relevant
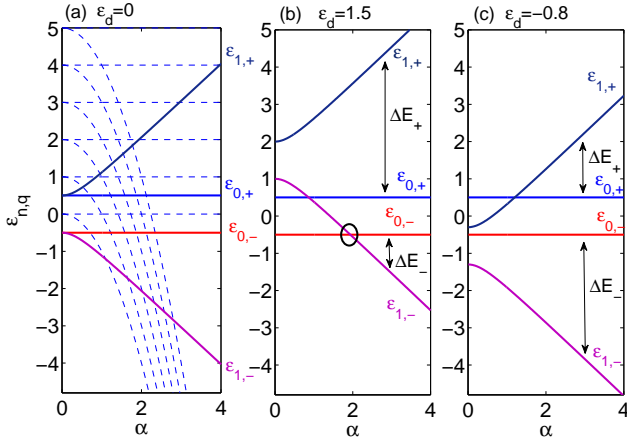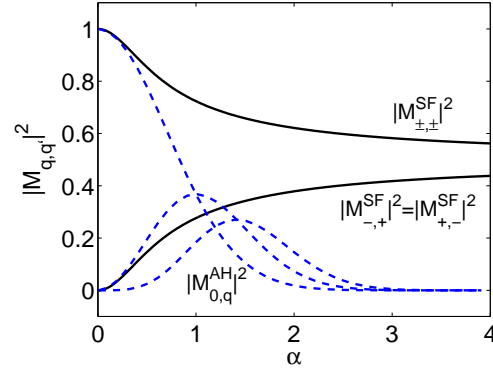
FIG. 2: Eigenenergies $\epsilon_{n,q}$ of the SF model (full) when (a) $\epsilon_d = 0$, (b) $\epsilon_d = 1.5$, and (c) $\epsilon_d = -0.8$. In panel (a) we also display low-lying ($q = 0, 1, ..., 5$) eigenenergies of the AH molecular Hamiltonian (dashed).

low temperature energy difference is given by

$$\Delta E_- \equiv |\epsilon_{1,-} - \epsilon_{0,-}|$$
$$= |\epsilon_d - \frac{\omega_0}{2}(\sqrt{1+4\alpha^2} - 1)|. \qquad (45)$$

Thermal effects may open up new channels, dramatically reducing the critical voltage: At high temperatures both spin states are occupied, thus three other transitions contribute to the current: This includes the transition involving the states $|1,+\rangle$ and $|0,+\rangle$, of spacing

$$\Delta E_+ \equiv |\epsilon_{1,+} - \epsilon_{0,+}|$$
$$= |\epsilon_d + \frac{\omega_0}{2}(\sqrt{1+4\alpha^2} - 1)|, \qquad (46)$$

and transitions which require a spin-flip (f),

$$\Delta E_\pm^f \equiv |\epsilon_{1,\pm} - \epsilon_{0,\mp}|$$
$$= |\epsilon_d \pm \frac{\omega_0}{2}(\sqrt{1+4\alpha^2} + 1)|. \qquad (47)$$

If $\epsilon_d < 0$ and α is taken sufficiently large, ΔE_+ becomes the smallest transition frequency, see Fig. 2(c). Thus, at *negative gating* the blockade region contracts from ΔE_- to ΔE_+ when we increase the temperature from $T_h/\omega_0 \ll 1$ to $T_h/\omega_0 \sim 1$. This strong effect is displayed below in Fig. 10.

(ii) The "Franck-Condon blockade" effect dominates the AH physics at strong electron-phonon coupling [6, 7]. This is because at large shifts $\alpha \gg 1$ transitions from $q = 0$ to high vibronic states ($q' >> q$) are favored over low-lying states, see the structure of the FC factors in Eq. (28). Thus, the (low-bias) current is suppressed and the blockade is lifted only at large bias once incoming electrons have sufficient energy to excite high vibronic states.

(iii) Repulsion (strength U) between electrons on the dot may drive the "Coulomb blockade" effect if $\Gamma_\nu < T_\nu$ and $U > \Gamma_\nu$. We do not consider this type of Blockade in the present analysis though extensions are immediate [23].

In what follows we exemplify current suppression in the AH and SF models. Recall that the Franck-Condon blockade physics is missing in the SF setup since its overlap matrix elements (29) do not cross. As a result, at weak electron-impurity coupling the transport behavior in the two models is expected to be similar, controlled by the ORB. At intermediate coupling (when the FC factors obey $|M_{0,0}| > |M_{0,1}| > |M_{0,2}|...$) both models are affected by the MB-ORB, renormalizing the suppression region. At strong coupling the AH model is controlled by the FC factors, while the behavior of the SF model is determined by the MB-ORB physics.

3. unequilibrated impurity

We display the current-voltage characteristics of the AH and the SF junctions in Figs. 5-6. The dot energy is
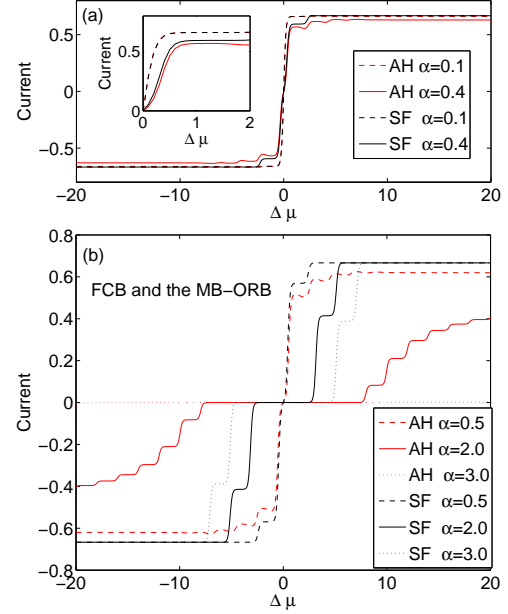

FIG. 5: Current-voltage characteristics of the AH and SF models at $\epsilon_d = 0$ with weak (a) and strong (b) electron-impurity coupling. (a) The inset zooms on weak coupling features, demonstrating the similarity, and onset of deviations, between the models, as coupling increases.

placed either at the center of the bias window, $\epsilon_d = 0$, or, under positive gating conditions we set $\epsilon_d = 1.5$ [54]. In the weak coupling limit ($\alpha \ll 1$) both models show similar features, particularly, an off-resonance suppression of the tunneling current, see Fig. 6(a). At strong coupling $\alpha \sim 2$, the models show current blockade, however the underlying cause differs. In the AH model the current is suppressed due to the behavior of the FC factors, favoring distant-energetic vibronic transitions; in the SF model diagonal, $q \to q$, transitions always dominate. Instead, the current is suppressed by the MB-ORB effect: As we increase the coupling to the impurity, the molecular frequency relevant for the onset of current develops as $\Delta E_- = |\epsilon_d - \frac{\omega_0}{2}(\sqrt{1+4\alpha^2} - 1)|$. When $\epsilon_d = 0$ the blockade region is monotonically increasing with α, in a linear fashion for large α. In the gated $\epsilon_d > 0$ case the blockade physics is more involved; the current is suppressed at sufficiently low biases if the bare energy ϵ_d is tuned *away* from the special point of degeneracy $\Delta E_- = 0$, satisfying

$$\epsilon_d = \frac{\omega_0}{2}\left(\sqrt{1+4\alpha^2} - 1\right). \qquad (48)$$

This point is encircled in Fig. 2(b), taking place at $\alpha = 1.94$ for $\epsilon_d = 1.5$. Fig. 6(c) shows that the low-bias current is indeed suppressed in the SF model when $\alpha \neq 1.9$.

Note that the MB-ORB effect takes place in the AH model as well: Besides the FC physics, the off-resonance blockade is lifted at level crossings when $\epsilon_{1,q} = \epsilon_{0,q}$, or $\epsilon_d = \alpha^2\omega_0$, see the $\alpha = 0.5, 1$ data lines in Fig. 6(b).
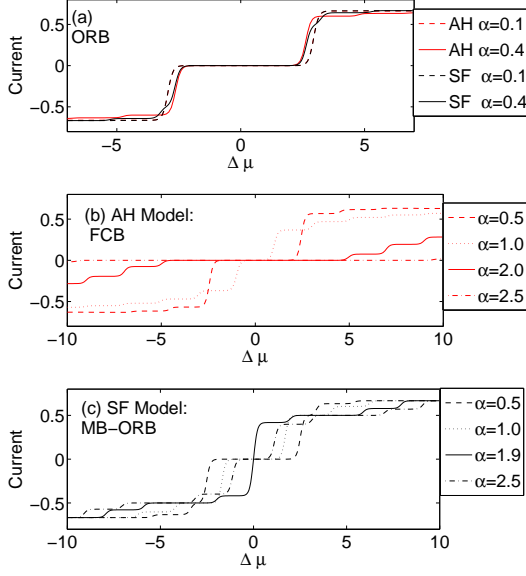
FIG. 6: Current-voltage characteristics in a gated $\epsilon_d = 1.5$ junction at weak (a) and strong (b-c) coupling. Different types of blockade play a role: (a) ORB at weak interactions, (b) FCB in the AH model, and (c) MB-ORB in the strongly-interacting SF model.

However, at large coupling ($\alpha > 1$) the MB-ORB effect is marginal in the AH model, and the FCB physics dominates.

Conductance plots ($dI/d\Delta\mu$) are presented in Fig. 7. The AH model demonstrates the FCB physics, the development of the gap with increasing α. The SF model shows uneven level spacings, the result of molecular anharmonicity, and the development of the MB-ORB effect away from the degeneracy point at $\Delta E_- = 0$. In Fig. 8 we complement this analysis and present the low-temperature conductance as a function of bias voltage and electron-impurity interaction parameter α. We find that at negative gating the blockade region monotonically increases with α. For positive gating there is a particular solution of Eq. (48), resulting in a resonance behavior.

4. Energy Dissipation and thermal equilibration

The behavior of the AH model with an equilibrated vibration was considered in several studies, see Refs. [6, 7, 11]. Models with explicit secondary heat baths were reviewed in Ref. [24]. In the context of the Franck-Condon blockade physics it was shown (in the sequential-tunneling regime) that the blockade becomes *more rigorous* when the harmonic mode is equilibrated; when the mode is unequilibrated tunneling electrons may leave the molecular system with an excited vibration, and subsequent tunneling processes can continue and increase the excitation state [6]. When co-tunneling processes are included, the AH model with equilibrated vibrations
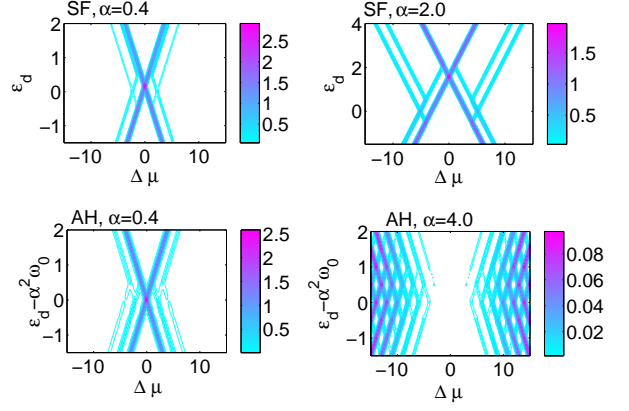

FIG. 7: Differential conductance plots of the SF (top) and the AH (bottom) models as a function of gate (ϵ_d) and applied bias voltage $\Delta\mu$ at weak and strong coupling, as indicated in the figure.
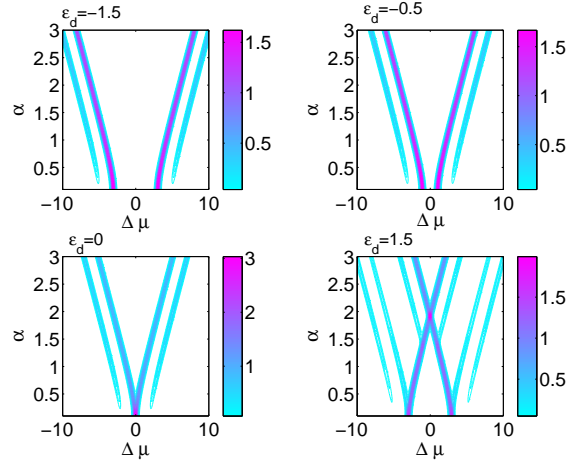

FIG. 8: Differential conductance plots of the SF model as a function of electron-spin interaction (α) and the bias voltage $\Delta\mu$ at different gating, as indicated in the figure.

shows a significant increase in current for small biases, $\Delta\mu < \alpha^2\omega_0$, yet the FCB survives.

In this section we study the role of dissipation effects and equilibration on the current-voltage characteristics of the SF model. The role of mode equilibration is explored using the ansatz (30). The more gentle introduction of dissipation effects is studied using Eqs. (32)-(40).

We found that the equilibration of the impurity did not affect the transport behavior of SF junctions when $\epsilon_d = 0$ (not shown). In Fig. 9 we thus display the current at positive gating, $\epsilon_d = 1.5$. First, we confirm that the dissipative model interpolates correctly between the isolated case $\Gamma_h = 0$ and the equilibrated $\Gamma_h/\omega_0 > \alpha$ limit. The latter choice of parameters goes beyond the weak (heat bath-impurity) coupling assumption underlying the derivation of Eq. (37). It is included here for demonstrating that the dissipative model provides seem-

ingly meaningful results even at strong dissipation Γ_h. It is interesting to note that coupling to a secondary bath may increase the current, compared to the case without this bath, or decrease it, see panel (b) in Fig. 9.

Thermal effects influence the current only modestly at positive gating as observed in Fig. 9, particularly leaving intact the MB-ORB region. This is true as long as ΔE_- is the smallest allowed transition frequency, see Fig. 2(b). In contrast, at negative gating ($\epsilon_d < 0$) dissipation or an enforced equilibration markedly influence the current, contracting the blockade region, see Fig. 10. As discussed below Eq. (46), this is because ΔE_+ is the smallest molecular frequency at negative gating and large α, see Fig. 2(c). Therefore, by thermally-occupying spin-up states we cut-down the critical voltage $\Delta\mu_c$ from ΔE_- to ΔE_+, further exposing the other $\Delta E_\pm^f$ transitions as steps in the current-voltage characteristics.

IV. ADIABATIC LIMIT $\Gamma_\nu > \omega_0$

In the previous section we studied the nonadiabatic high temperature limit, $\Gamma_\nu < \omega_0, T_\nu$, while allowing the electron-impurity interaction energy to become arbitrary large. In this section we focus on the opposite adiabatic regime of large tunneling elements $\Gamma_\nu > \omega_0$, small α, and low temperatures $T_\nu < \omega_0$.

The possible existence of more than one steady-state in molecular junctions, and potential mechanisms of bistability, switching, and hysteresis, have been topics of interest and controversy in the past decade. While early considerations adopted the Born-Oppenheimer mean-field approximation [14, 18] and perturbative treatments [15], more recent studies addressed this problem using brute-force numerically exact simulation tools [19, 20, 30].

In this section we consider the existence of bistability, hysteresis and switching in molecular junctions con-
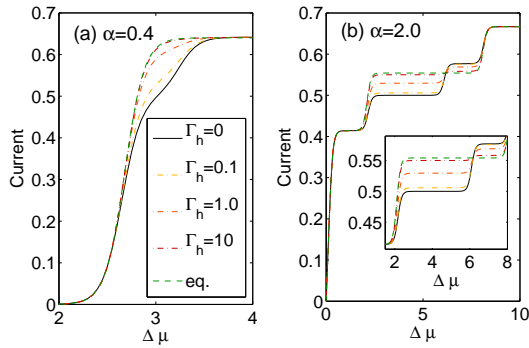

FIG. 9: Mild effect of mode equilibration on the current at $\epsilon_d > 0$ in the (a) weak coupling limit, and (b) at strong coupling; the inset zooms on the region of interest. The legend describes all panels: (full) excluding a heat bath, (dashed-dotted lines) including a dissipative spin bath at different couplings, and (dashed) once enforcing impurity equilibration as in Eq. (30). We used $\epsilon_d = 1.5$ and $T_h = 0.05$.
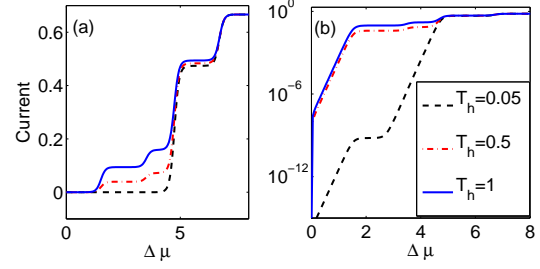

FIG. 10: Strong influence of mode equilibration on the current at $\epsilon_d < 0$ (a) linear scale, (b) logarithmic scale, displaying steps at low temperatures. The temperature of the electronic baths is (as before) $T_\nu = 0.05$. T_h is indicated in the figure, and we used $\alpha = 2$ and $\epsilon_d = -0.8$.

sisting an anharmonic impurity, the SF model. These effects, discussed so far in detail within the AH model, are in principle not limited to strictly harmonic impurities. Our analysis goes back to the simple mean-field treatment of Galperin et al. [14] valid in the limit of a large tunneling element $\Gamma_\nu > \omega_0$. This mean-field approach naturally fails in certain physical regimes [16, 17], yet it serves as a valid starting point for comparing the AH and SF models, for considering phenomenology preceding extensive numerical treatments [19, 20]. We find that the self-consistent equations, for the dot occupation and charge current, have a related form in the AH and SF models. However, bistability and hysteresis are missing in the latter case, considering the allowed-consistent range of parameters.

We begin by introducing a variant of the dissipative SF model, complementing the models of Sec. III B,

$$
\begin{aligned}
H_{SF}^{diss} &= \sum_{\nu,k} \epsilon_k a_{\nu,k}^\dagger a_{\nu,k} + \sum_{\nu,k} \left(v_{\nu,k} a_{\nu,k}^\dagger d + v_{\nu,k}^* d^\dagger a_{\nu,k} \right) \\
&+ \epsilon_d \hat{n}_d + \frac{\omega_0}{2}\sigma_z + \alpha\omega_0\sigma_x\hat{n}_d \\
&+ \sum_j \omega_j b_j^\dagger b_j + \sigma_z \sum_j \eta_j \left(b_j^\dagger + b_j \right).
\end{aligned}
\tag{49}
$$

The impurity polarization is coupled to displacements of harmonic oscillators in a secondary heat bath, itself prepared in a thermodynamic state at temperature T_h. In the adiabatic limit $\Gamma_\nu > \omega_0$ tunneling electrons are fast and the two-state impurity is slow. Under a Born-Oppenheimer timescale-separation approximation a dissipative spin Hamiltonian can be defined,

$$
\begin{aligned}
H_S &= \frac{\omega_0}{2}\sigma_z + M\sigma_x n_d \\
&+ \sum_j \omega_j b_j^\dagger b_j + \sigma_z \sum_j \eta_j \left(b_j^\dagger + b_j \right),
\end{aligned}
\tag{50}
$$

consisting slow DOF. Here $n_d = \mathrm{tr}[\rho\hat{n}_d]$ stands for the expectation value of the dot number operator in the steady-state limit; ρ is the total density matrix. The definition $M \equiv \alpha\omega_0$ for the electron-spin interaction energy takes

us back to the notation of Ref. [14]. However, while in the AH model the related electron-averaged Hamiltonian includes only harmonic modes, resulting in an exact quantum Langevin equation treatment [14], Eq. (50) reduces to the more complex "spin-boson" Hamiltonian; by further defining the spin tunneling element as $\Delta \equiv 2Mn_d$ we recover the usual form of this model.

It is useful to define the spectral density function, $J(\omega) = 4\pi \sum_j \eta_j^2 \delta(\omega - \omega_j)$, enclosing the interaction of the spin with the boson heat bath. It is assumed here to take an Ohmic form,

$$J(\omega) = 2\pi\omega K e^{-\omega/\omega_c}, \tag{51}$$

with ω_c as the cutoff frequency of the heat bath and K a dimensionless damping parameter.

The thermodynamic properties and the dynamical behavior of the spin-boson model were explored in details in different limits [55]. If the damping is weak ($K \ll 1$) it can be shown that the long-time bath-traced coherence obeys in the Ohmic case the expression

$$\langle \sigma_x \rangle \sim -\frac{\Delta_{eff}^2}{\Delta\Omega} \tanh \frac{\Omega}{2T_h}, \tag{52}$$

valid beyond the noninteracting blip approximation [55]. Here $\Omega^2 = \Delta_b^2(1 + 2K\mu)$, $\Delta_b = [\omega_0^2 + \Delta_{eff}^2]^{1/2}$, $\mu = \Re\Psi(i\Delta_b/2\pi T_h) - \ln(\Delta_b/2\pi T_h)$ with $\Re$ denoting the real part of ψ, the digamma function. The effective tunneling element, between spin states, is given by $\Delta_{eff} = \Delta [\Gamma(1 - 2K)\cos(\pi K)]^{1/2(1-K)} (\Delta/\omega_c)^{K/(1-K)}$; Γ stands here for the Gamma function [55]. While we could continue our analysis with this expression, we simplify it so as to arrive at the expressions of Ref. [14]. We thus consider the limits $\omega_c \gg \Delta$, $\omega_0 > \Delta$, and $T_h < \Delta$. We can now approximate $\Delta_{eff} \to \Delta$, $\Delta_b \to \omega_0$, reducing Eq. (52) to

$$\langle \sigma_x \rangle \sim -\frac{\Delta}{\omega_0(1 + K\mu)}, \tag{53}$$

recall that $\Delta = 2Mn_d$. The denominator describes the renormalization of the spin splitting due to the coupling to a heat bath. We now turn our attention to the fast, fermionic, degrees of freedom, and define the Hamiltonian

$$H_F \equiv \tilde{\epsilon}_d(n_d)\hat{n}_d + \sum_{\nu,k} \epsilon_k a_{\nu,k}^\dagger a_{\nu,k}$$
$$+ \sum_{\nu,k} \left(v_{\nu,k} a_{\nu,k}^\dagger d + v_{\nu,k}^* d^\dagger a_{\nu,k} \right), \tag{54}$$

with the shifted dot energy

$$\tilde{\epsilon}_d(n_d) = \epsilon_d - \frac{2M^2 n_d}{\omega_0(1 + K\mu)}. \tag{55}$$

The shift is referred to as a "reorganization energy", $\epsilon_{reorg} \equiv M^2/[\omega_0(1 + K\mu)]$, and it absorbs the response of

the impurity and its attached bath to charge occupation on the dot.

The electronic Hamiltonian, Equations (54)-(55), is parallel to the result of Galperin et al. [14]. Repeating their arguments, bistability may, in principle, develop since the following coupled equations can take more than one solution,

$$n_d = \frac{\Gamma_L}{\pi(\Gamma_L + \Gamma_R)} \arctan\left[x + 2\frac{\mu_L}{(\Gamma_L + \Gamma_R)}\right]$$
$$+ \frac{\Gamma_R}{\pi(\Gamma_L + \Gamma_R)} \arctan\left[x + 2\frac{\mu_R}{(\Gamma_L + \Gamma_R)}\right]$$
$$+ \frac{1}{2}, \tag{56}$$
$$n_d = \frac{\Gamma_L + \Gamma_R}{4\epsilon_{reorg}}x + \frac{\epsilon_d}{2\epsilon_{reorg}}, \tag{57}$$

The first equation here describes the steady-state zero-temperature expectation value of the dot occupation under the electronic Hamiltonian (54). The second equation corresponds to the shifted dot energy (55) with ($\mu_F = (\mu_L + \mu_R)/2 = 0$) $x \equiv -2\tilde{\epsilon}_d/(\Gamma_L + \Gamma_R)$. To treat the case of nonzero temperatures one should retract to Eq. (52) and employ the finite temperature solution for the dot occupation, replacing Eq. (56).

We now point that in developing Eq. (55) we have made the assumption $\Delta < \omega_0$, translating to $\alpha < 1$. Given that $\Gamma_\nu > \omega_0$, we conclude that our analysis is valid only when $\epsilon_{reorg} \sim \alpha^2\omega_0 < \Gamma_\nu$. This implies a large slope in Eq. (57), providing only one solution, see Fig. 11. It can be similarly shown that multiple solutions are missing in the opposite $\Delta > \omega_0$ limit.

Thus, when the electron is coupled to a dissipative two-state mode, we reach adiabatic equations which directly correspond to those obtained in the dissipative AH model. However, multiple solutions are missing in the SF model at the level of the mean-field approximation. Numerically exact simulations should be performed to reach conclusive results. Particularly fitting are influence functional path integral approaches in which the impurity spectrum is naturally truncated [56].

To complement transport studies, Sec. III, we further write the adiabatic limit of the charge current, a Landauer expression,

$$I = \frac{1}{2\pi} \int d\epsilon \frac{\Gamma_L\Gamma_R[f_L(\epsilon) - f_R(\epsilon)]}{[\epsilon - \tilde{\epsilon}_d(n_d)]^2 + (\Gamma_L + \Gamma_R)^2/4}. \tag{58}$$

The (assumed energy independent) hybridization energy Γ_ν was defined in Eq. (5). The system shows an off-resonance blockade, and the critical bias is (simply) linearly reduced by the reorganization energy, see Eq. (55).

V. SUMMARY

The Anderson-Holstein model provides a minimal description of molecular junctions, by including the in-
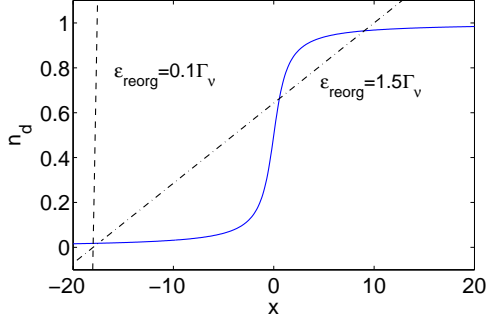
FIG. 11: Electronic dot occupation in the SF model, quantum adiabatic limit, with $\epsilon_d = 4.5$, $\Delta\mu = 0$, and $\Gamma_\nu = 0.25$. The full line was generated from Eq. (56). Eq. (57) provides the dashed (dashed-dotted) lines, based on data consistent (inconsistent) with the derivation of Eq. (57); the dashed-dotted line is included here for demonstrating that multiple solutions can show only when $\epsilon_{reorg}/\Gamma > 1$, deviating from the assumptions leading to Eq. (57).

teraction of electrons in the molecule with a harmonic-vibrational mode. The spin-fermion model describes simplified nonequilibrium Kondo-like systems in which conducting electrons interact with a spin impurity. Our goal here has been to complement studies of the AH model, and analyze the role of mode anharmonicity on nonlinear transport characteristics, blockade physics and possible bistability.

In the first - main part of the paper we considered the nonadiabatic (slow electron) limit. We transformed the AH and the SF models into a comparable form, suitable for a perturbative expansion in the tunneling element, where to that order, the coupling of the dot electron to the impurity (vibrational mode or spin) is included to all orders. In the limit of weak electron-impurity coupling the two models support similar transport behavior. At strong electron-impurity interactions significant deviations arise. Principally, the SF model does not support the analog of the Franck Condon blockade physics which governs the behavior of the AH model. However, the SF model does show a nontrivial many-body off-resonance current suppression; the off-resonance regime is determined by a nonlinear function of the electron coupling to the impurity, and by the gate voltage ($\epsilon_d \neq 0$). In the second part of the paper we briefly analyzed the adiabatic limit at low temperatures. Based on mean-field arguments, we pointed out that that electron occupation and the charge current in the SF model obey adiabatic equations analogous to those reached in the AH system. However, multiple solutions are absent in the case of a two-state impurity, thus nonlinear transport effects such as bistability and hysteresis are missing, at this level of approximation.

The AH and the SF models discussed in this paper can describe hybrid physical scenarios beyond molecular

junctions [57], for example, nanomechanical systems in which the conducting electrons interact with mechanical modes [9], and *photon* assisted electron transport situations, through quantum dot systems [58]. In future work we will examine the correspondence in transport behavior between harmonic and anharmonic-mode models using numerically exact methodologies [56].

Appendix: Collections of harmonic modes or spins

The general transformation discussed in Sec. II A can be performed on an extended model with M spin-degenerate electronic sites, $m = 1, 2, ..., M$, where each site is coupled to multiple impurities. In the case of the generalized AH model this constitutes a collection of phonons, and the tight-binding network is given by

$$H_{AH}^M = \sum_m \epsilon_m \hat{n}_m + \sum_{m,m'} \left(v_{m,m'} a_m^\dagger a_{m'} + v_{m',m}^* a_{m'}^\dagger a_m \right) + \sum_p \omega_p b_p^\dagger b_p + \sum_m \hat{n}_m \sum_p \alpha_{m,p} \omega_p \left(b_p^\dagger + b_p \right). \quad (A1)$$

Here $a_m^\dagger$ (a_m) are creation (annihilation) fermionic operators. The set of local phonons (creation operator $b_p^\dagger$) is coupled to the electronic number operator of site m, $\hat{n}_m$, with the dimensionless parameter $\alpha_{m,p}$. The polaron-transformed Hamiltonian, an extension of Eq. (14), is given by

$$\bar{H}_{AH}^M = \sum_m \left(\epsilon_m - \sum_p \alpha_{m,p}^2 \omega_p \right) \hat{n}_m + \sum_{m,m'} \left(v_{m,m'} a_m^\dagger a_{m'} e^{(A_m - A_{m'})} + h.c. \right) + \sum_p \omega_p b_p^\dagger b_p, \quad (A2)$$

with the anti-hermitian operator $A_m = \sum_p \alpha_{m,p}(b_p^\dagger - b_p)$. The rate constant of electron hopping between neighboring sites can be calculated e.g., by treating $v_{m,m'}$ as a small parameter [59]. Recent studies adopted this model for describing coherent electronic energy transfer in a protein environment, see for example Refs. [47, 48].

Equation (A1) has been often introduced in the literature to model the interaction of electrons or excitons with a normal-mode environment (phonons, photons),

but a local-anharmonic spin-bath can be similarly implemented. The M-site SF model is given by the Hamiltonian

$$
\begin{aligned}
H_{SF}^M &= \sum_m \epsilon_m \hat{n}_m + \sum_{m,m'} \left(v_{m,m'} a_m^\dagger a_{m'} + v_{m',m}^* a_{m'}^\dagger a_m \right) \\
&+ \sum_p \frac{\omega_p}{2} \sigma_z^p + \sum_m \hat{n}_m \sum_p \alpha_{m,p} \omega_p \sigma_x^p.
\end{aligned}
\tag{A3}
$$

The spin bath includes many local modes of spacing ω_p, described by the Pauli matrices $\sigma_{x,y,z}^p$, coupled via $\alpha_{m,p}$ to the electronic number operator on site m. This Hamiltonian can be transformed by extending the procedure of Sec. II C to receive

$$
\begin{aligned}
\bar{H}_{SF}^M &= \sum_m \epsilon_m \hat{n}_m + \sum_{m,m'} \left(v_{m,m'} a_m^\dagger a_{m'} e^{(A_m - A_{m'})} + h.c. \right) \\
&+ \sum_p \frac{\omega_p}{2} \sigma_z^p + \sum_m \hat{n}_m \sum_p \frac{\omega_p}{2} \left(\frac{1 - \cos 2\lambda_{m,p}}{\cos 2\lambda_{m,p}} \right) \sigma_z^p.
\end{aligned}
\tag{A4}
$$

Here $\lambda_{m,p} = \frac{1}{2} \arctan(2\alpha_{m,p})$ is a renormalized coupling parameter and $A_m = i \sum_p \lambda_{m,p} \sigma_y^p$ is the anti-hermitian operator generating the transformation. It is interesting to extend recent polaron studies of exciton transfer in biomolecules and examine the dynamics under the local-bath model (A4), to understand the role of bath harmonicity/anharmonicity (normal modes or local modes) in sustaining quantum coherent dynamics of electronic degrees of freedom.

[1] D. Natelson, ACS Nano **6**, 2871 (2012).
[2] J. P. Bergfield and M. A. Ratner, Phys. Stat. Solidi B **250**, 2249 (2013), and references therein.
[3] S. Aradhya and L. Venkataraman, Nature Nano. **8**, 399 (2013), and references therein.
[4] W. Wang, T. Lee, I. Kretzschmar, and M. A. Reed, Nano Lett. **4**, 643 (2004).
[5] D. R. Ward, D. A. Corley, J. M. Tour, and D. Natelson, Nature Nano. **6**, 33 (2011).
[6] J. Koch and F. von Oppen, Phys. Rev. Lett. **94**, 206804 (2005).
[7] J. Koch, F. von Oppen, and A. V. Andreev, Phys. Rev. B **74**, 205438 (2006).
[8] M. C. Lüffe, J. Koch, and F. von Oppen, Phys. Rev. B **77**, 125305 (2008).
[9] R. Leturcq, C. Stampfer, K. Inderbitzin, L. Durrer, C. Hierold, E. Mariani, M. G. Schultz, F. von Oppen, and K. Ensslin, Nature Phys. **5**, 327 (2009).
[10] J. Koch, M. Semmelhack, F. von Oppen, and A. Nitzan, Phys. Rev. B **73**, 155306 (2006).
[11] A. Mitra, I. Aleiner, and A. J. Millis, Phys. Rev. B **69**, 245302 (2004).
[12] R. Härtle and M. Thoss, Phys. Rev. B **83**, 125419 (2011).
[13] R. Härtle and M. Thoss, Phys. Rev. B **83**, 115414 (2011).
[14] M. Galperin, M. A. Ratner, and A. Nitzan, Nano Lett. **5**, 125 (2005).
[15] M. Galperin, A. Nitzan, and M. A. Ratner, J. Phys.: Condens. Matter **20**, 374107 (2008).
[16] A. S. Alexandrov and A. M. Bratkovsky, J. Phys.: Condens. Matter **19**, 255203 (2007).
[17] A. S. Alexandrov and A. M. Bratkovsky, Phys. Rev. B **80**, 115321 (2009).
[18] A. A. Dzhioev and D. S. Kosov, J. Chem. Phys. **135**, 174111 (2011).
[19] E. Y. Wilner, H. Wang, G. Cohen, M. Thoss, and E. Rabani, Phys. Rev. B **88**, 045137 (2013).
[20] E. Y. Wilner, H. Wang, M. Thoss, and E. Rabani, arXiv:1402.6454.
[21] J. Koch, M. E. Raikh, and F. von Oppen, Phys. Rev. Lett. **96**, 056803 (2006).
[22] D. Segal, A. Nitzan, W. B. Davis, M. R. Wasielewsky, and M. A. Ratner, J. Phys. Chem. B **104**, 3817 (2000).
[23] J. Koch, F. von Oppen, Y. Oreg, and E. Sela, Phys. Rev. B **70**, 195107 (2004).
[24] M. Galperin, M. A. Ratner, and A. Nitzan, J. Phys.: Condens. Matter **19**, 103201 (2007).
[25] H. Wang, I. Pshenichnyuk, R. Härtle, and M. Thoss, J. Chem. Phys. **135**, 244506 (2011).
[26] A. Jovchev and F. B. Anders, Phys. Rev. B **87**, 195112 (2013).
[27] E. Eidelstein, D. Goberman, and A. Schiller, Phys. Rev. B **87**, 075319 (2013).
[28] R. Hützen, S. Weiss, M. Thorwart, and R. Egger, Phys. Rev. B **85**, 121408(R) (2012).
[29] P. Werner, T. Oka, M. Eckstein, and A. J. Millis, Phys. Rev. B **81**, 035108 (2010).
[30] K. F. Albrecht, A. Martin-Rodero, R. C. Monreal, L. Mühlbacher, and A. L. Yeyati, Phys. Rev. B **87**, 085127 (2013).
[31] J. Koch and F. von Oppen, Phys. Rev. B **72**, 113308 (2005).
[32] L. Bogani and W. Wernsdorfer, Nature Mat. **7**, 179 (2008).
[33] W. Liang, M. P. Shores, M. Bockrath, J. R. Long, and H. Park, Nature **417**, 725 (2002).
[34] H. Park, J. Park, A. K. L. Lim, E. H. Anderson, A. P. Alivisatos, and P. L. McEuen, Nature **407**, 57 (2000).
[35] C. Lopez-Monis, C. Emary, G. Kiesslich, G. Platero, and T. Brandes, Phys. Rev. B **85**, 045301 (2012).
[36] K. Mosshammer, G. Kiesslich, and T. Brandes, Phys. Rev. B **86**, 165447 (2012).
[37] A. Metelmann and T. Brandes, Phys. Rev. B **86**, 245317

(2012).

[38] G. Balasubramanian, I. Y. Chan, R. Kolesov, M. Al-Hmoud, J. Tisler, C. Shin, C. Kim, A. Wojcik, P. R. Hemmer, A. Krueger, T. Hanke, A. Leitenstorfer, R. Bratschitsch, F. Jelezko, and J. Wrachtrup, Nature **455**, 648 (2008).

[39] J. R. Maze, P. L. Stanwix, J. S. Hodges, S. Hong, J. M. Taylor, P. Cappellaro, L. Jiang, M. V. Gurudev Dutt, E. Togan, A. S. Zibrov, A. Yacoby, R. L. Walsworth, and M. D. Lukin, Nature **455**, 644 (2008).

[40] L. Venkataraman, J. E. Klare, C. Nuckolls, M. S. Hybertsen, and M. L. Steigerwald, Nature **442**, 904 (2006).

[41] G. D. Mahan, *Many-particle physics* (Plenum press, New York, 2000).

[42] A. Mitra and A. J. Millis, Phys. Rev. B **72**, 121102(R) (2005).

[43] D. Segal, D. R. Reichman, and A.J. Millis, Phys. Rev. B **76**, 195316 (2007).

[44] D. Segal, A. J. Millis, and D. R. Reichman, Phys. Rev. B **82**, 205323 (2010).

[45] R. M. Lutchyn, L. Cywinski, C. P. Nave, and S. Das Sarma, Phys. Rev. B **78**, 024508 (2008).

[46] D. Segal, J. Chem. Phys. **140**, 164110 (2014).

[47] S. Jang, Y.-C. Cheng, D. R. Reichman, and J. D. Eaves, J. Chem. Phys. **129**, 101104 (2008).

[48] A. Kolli, A. Nazir, and A. Olaya-Castro, J. Chem. Phys. **135**, 154112 (2011).

[49] H.-P. Breuer and F. Petruccione, *The Theory of Open Quantum Systems* (Oxford University Press, New York, New York, 2002).

[50] Depending on the model, the quantum master equation may be derived by defining a new molecular Hamiltonian $\bar{H}'_S = \bar{H}_S + \text{tr}_B[\bar{H}_{SB}]$ and a corresponding interaction term $\bar{H}'_{SB} = \bar{H}_{SB} - \text{tr}_B[\bar{H}_{SB}]$. This choice enforces offsetting of the first-order term in the perturbative expansion, $\text{tr}_B[\bar{H}'_{SB}] = 0$.

[51] A. Nitzan, *Chemical Dynamics in Condensed Phases* (Oxford Graduate Texts 2006).

[52] S. Maier, T. L. Schmidt, and A. Komnik, Phys. Rev. B **83**, 085401 (2011).

[53] Y. Utsumi, O. Entin-Wohlman, A. Ueda, and A. Aharony, Phys. Rev. B **87**, 115407 (2013).

[54] Fig. 5 was generated with the same parameters as Fig. 1(a) Ref. [6], but here, we set the bare energy as $\epsilon_d = 0$, so as to allow a clear comparison to the SF model. In contrast, in Ref. [6] the renormalized energy was fixed, $\epsilon_d - \alpha^2 \omega_0 = 0$. Our AH results match Ref. [6] when we follow their convention.

[55] U. Weiss, *Quantum Dissipative Systems* (World Scientific, Singapore, 1993).

[56] L. Simine and D. Segal, J. Chem. Phys. **138**, 214111 (2013).

[57] Z.-L. Xiang, S. Ashhab, J. Q. You, and F. Nori, Rev. Mod. Phys. **85**, 623 (2013).

[58] V. Gudmundsson, O. Jonasson, C.-S. Tang, H.-S. Goan, and A. Manolescu, Phys. Rev. B **85**, 075306 (2012).

[59] R. Silbey and R. A. Harris, J. Chem. Phys. **80**, 2615 (1984); R. A. Harris and R. Silbey, *ibid.* **83**, 1069 (1985); A. Suarez and R. A. Silbey, *ibid.* **94**, 4809 (1991).